Study of the Formation of the First Aromatic Rings in the Pyrolysis of Cyclopentene

Olivier Herbinet, Anne Rodriguez, Benoit Husson, Frédérique Battin-Leclerc, Zhandong Wang, Zhanjun Cheng, Fei Qi

Study of the Formation of the First Aromatic Rings in the Pyrolysis of Cyclopentene

Olivier Herbinet[1,2,*], Anne Rodriguez[1,2], Benoit Husson[1,2], Frédérique Battin-Leclerc[1,2], Zhandong Wang[3], Zhanjun Cheng[3], and Fei Qi[3]

[1] Laboratoire Réactions et Génie des Procédés, Université de Lorraine, UMR 7274, BP 20451, 1 rue Grandville, Nancy, F-54000, France
[2] Laboratoire Réactions et Génie des Procédés, CNRS, UMR 7274, BP 20451, 1 rue Grandville, Nancy, F-54000, France
[3] National Synchrotron Radiation Laboratory, University of Science and Technology of China, Hefei, Anhui 230029, P. R. China

Article published in J. Phys. Chem. A, 2016, 120 (5), pp 668–682

Abstract

The thermal decomposition of cyclopentene was studied in a jet-stirred reactor operated at constant pressure and temperature to provide new experimental information about the formation of the first aromatic rings from cyclic C_5 species. Experiments were carried out at a residence time of 1 s, a pressure of 106.7 kPa, temperatures ranging from 773 to 1073 K and under diluted conditions (cyclopentene inlet mole fraction of 0.04). Species were quantified using three analytical methods: gas chromatography, synchrotron vacuum ultraviolet photoionization mass spectrometry (SVUV-PIMS), and single photon laser ionization mass spectrometry (SPI-MS). Several species could be quantified using both methods allowing comparison of experimental data obtained with the three apparatuses. Discrepancies observed in mole fraction profiles of some large aromatics suggest that the direct sampling in the gas phase (with a molecular beam or a capillary tube) provide more reliable results. The main reaction products are 1,3-cyclopentadiene and hydrogen. The formation of many unsaturated C_2–C_6 olefins, diolefins and alkynes was also observed but in smaller amounts. Benzene, toluene, styrene, indene, and naphthalene were detected from 923 K. SVUV-PIMS data allowed the identification of another C_6H_6 isomer which is 1,5-hexadien-3-yne rather than fulvene. The quantification of the cyclopentadienyl radical was obtained from SVUV-PIMS and SPI-MS data with some uncertainty induced by the possible contribution to the signal for *m/z* 65 of a fragment from the decomposition of a larger ion. This is the first time that a radical is quantified in a jet-stirred reactor using non-optical techniques. SPI-MS analyses allowed the detection of species likely being combination products of allyl and cyclopentadienyl radicals. A model was developed for the pyrolysis of cyclopentene. This model includes routes of formation of aromatics from the cyclopentadienyl radical. The comparison of experimental and computed data is overall satisfactory for primary reaction products whereas discrepancies are still observed for aromatics.

Introduction

The chemistry involved in the formation of small aromatics, which is the first step toward soot formation, has been the subject of numerous studies. However, there are still uncertainties in the numerous formation pathways and associated kinetic parameters.[1,2] Some of these studies suggest that the growing of aromatics relies not only on the reactions of small C_2–C_4 species but also on those of C_5 species such as the cyclopentadienyl radical.[1,2]

There are very little data about the pyrolysis of cyclic C_5 hydrocarbons such as cyclopentene and 1,3-cyclopentadiene in the literature. Cyclopentene pyrolysis studies mainly aimed at measuring the kinetic parameters of the reaction of decomposition of this fuel to 1,3-cyclopentadiene and hydrogen (e.g., ref 3). There are more data about the oxidation of 1,3-cyclopentadiene. Most of these studies were performed under high temperature conditions (e.g., refs 4−10). They consisted in measuring ignition delay times[4] or studying flat flame structures to understand the formation of aromatics.[5-10] All of these studies showed that the C_5 species are of importance in the formation of aromatics (as an example the formation of toluene can be explained from the reaction between the cyclopentadienyl radical and acetylene according to the model developed by[9]) even if there is still no definitive agreement about the chemistry which is involved in their formation.

The pyrolysis of 1,3-cyclopentadiene was also studied in a tubular flow reactor with products analyses.[11-13] Kim et al. performed a study at temperatures ranging from 823 to 1223 K, a residence time of 3 s, atmospheric pressure and fuel inlet mole fraction of 0.007 (dilution in N_2).[11,12] Major products were benzene, indene and naphthalene. The observation of species such as methyl-indene and dihydro-naphthalene intermediates suggested that recombination of cyclopentadienyl radicals could be a dominant pathway in the formation of indene and naphthalene. Djokic et al. studied the pyrolysis of 1,3-cyclopentadiene in a tubular flow reactor over the temperature range 873–1123 K, at residence times in the range 300–400 ms, at a pressure of 1.7 bar and at two fuel inlet mole fractions: 0.04 and 0.17 (dilution in N_2).[13] Many reaction products were observed, the major ones being benzene, indene, methyl-indenes and naphthalene. The kinetic analysis of the model developed in this work showed that reactions of combination and addition of cyclopentadienyl radicals are very sensitive in the formation of the first aromatics.

Quantum mechanical studies have also been performed to elucidate the formation of aromatics from the cyclopentadienyl radical.[14-18] As an example Cavalotti et al. suggest a fast formation of toluene and benzene from the addition of the cyclopentadienyl radical to acetylene.[16] More recently, Kislov and Mebel proposed a comprehensive study of the formation of naphthalene, azulene and fulvalene from cyclic C_5 species.[17] All these theoretical studies showed that the formation of aromatics and polyaromatics is a complex phenomenon which involves many possible pathways, the sensibility of which depends on the composition of the gas phase and thus of the structure of the initial fuel which is burned.

The goal of the present study is to investigate the reaction of cyclopentene under pyrolysis conditions at relatively low temperatures in a type of reactor which is well adapted to kinetic studies to catch the primary reaction chemistry which is involved in the formation of the first aromatics from C_5 species. Three types of analytical methods were used to detect a wide range of intermediates: gas chromatography (GC), synchrotron vacuum ultraviolet photoionization mass spectrometry (SVUV-PIMS), and single photon laser ionization mass spectrometry (SPI-MS). Experimental data obtained with the three analytical techniques were compared to highlight possible discrepancies due to the sampling method. A model for the pyrolysis of cyclopentene including a new chemistry set based on literature review for the formation of aromatics

from the cyclopentadienyl radical was developed and tested against experimental data obtained in the present study.

Experimental Methods

Experiments were carried out in a fused silica jet-stirred reactor which can be modeled as a perfectly stirred reactor. This type of reactor has already been used for pyrolysis and oxidation studies.[19-23] This reactor was designed by following rules recommended by Matras, David, and Villermaux.[24,25] They showed that their reactor enabled to obtain a good macro mixing from their residence time distribution measurements.[24] A preheating with an annular geometry was added to the reactor to progressively heat the mixture up to the reactor temperature in a very short period of time. This helps maintaining the homogeneity of the temperature in the gas phase inside the reactor.[26]

The reactor is a quartz sphere (volume = 90 cm^3). The reactant and carrier gas enter through an injection cross located at its center. The gas jets provoke high turbulence leading to homogeneity in composition and temperature of the gas phase. Gas flow rates were controlled by mass flow controllers, Coriolis flow controllers were used for cyclopentene. The uncertainty in the flow measurements is around 0.5% for each controller. This results in a maximum uncertainty of about ±5% in the residence time (τ = 1 ± 0.05 s in the present work).

Both the spherical reactor and the annular preheating zone are heated by heating resistances rolled up around their walls in Nancy. In Hefei, because of the lateral sampling cone, it was not possible to use heating resistances for the heating of the spherical part. A special oven with the same shape as the reactor (sphere and cone) was designed and used for the heating.[27] In both laboratories, the reaction temperature was measured with a type K thermocouple inserted in the intra-annular part of the preheater (the extremity of the thermocouple is located at the center of the reactor in a glass finger in the injection cross). The accuracy of the reaction temperature with the two types of heating device was ±5 K.

Three methods were used to analyze reaction products. Online gas chromatography and single photon laser ionization mass spectrometry were used in France, and synchrotron vacuum ultraviolet photoionization mass spectrometry with direct sampling through a molecular jet was used in China. A schematic diagram of the two mass spectrometry methods is displayed in Figure S1. Helium was used as carrier gas in France whereas argon was required in China as the signal recorded for this species was used as reference for the normalization of other signals.

In France, helium was provided by Messer (with a purity reported as 99.999%) and cyclopentene was provided by Sigma-Aldrich (purity of 99%). In China, argon was provided by Nanjing Special Gas Factory Co.,Ltd. (with a purity was 99.99%) and cyclopentene was purchased from Aladdin Reagent Co.,Ltd. with a purity of 99%.

Gas Chromatography Analysis

This method provides the advantages of an easy separation of different isomers, a high sensitivity, and an easy and direct quantification of species but it is not suitable to analyze unstable species as they decompose before the analysis. Analyses were performed online thanks a heated transfer line connecting the outlet of the reactor to the three gas chromatographs that were used for the quantification of a large range of reaction products. Gas chromatographs were fitted with 6 way valves including an injection loop of 250 µL. The transfer line was a chromatography quality cooper tube (inside diameter of 4.83 mm). It was heated up to 423 K.

The first gas chromatograph, equipped with a Carbosphere packed column, a thermal conductivity detector (TCD), and a flame ionization detector (FID), was used for the quantification of hydrogen. The temperature of the oven was 303.15 K during 10 min. The carrier gas was argon to have a good sensitivity for H_2 (25 mL·min^{-1}, constant pressure, splitless). The second one was fitted with a PlotQ capillary column and a FID, and was used for the quantification of molecules from methane to reaction products containing up to 5 carbon atoms. The temperature profile was: 333.15 K during 10 min–ramp of 5 K·min^{-1} up to 623.15–623.15 K during 15 min. The carrier gas was helium (2 mL·min^{-1}, constant flow, split 1/10). The third one was fitted with a HP-5 capillary column and a FID and was used for the quantification of molecules which contain at least 5 carbon atoms. The temperature profile was as follows: 313.15 K during 30 min; ramp of 5 K·min^{-1} up to 573.15–573.15 K during 8 min. The carrier gas was helium (1 mL·min^{-1}, constant flow, split 1/10).

Calibration was performed by injecting standards when available or by using the effective carbon number method (only applicable with the flame ionization detector) when not available. Maximum relative uncertainty in mole fractions was estimated as ±5% for species calibrated using standards and ±10% for species calibrated using the carbon effective number methods (with error bars shown in Figure 1). The limit of detection for species was about 1 ppm for species analyzed using flame ionization detector and 1000 ppm for hydrogen analyzed using thermal conductivity detector. Reaction products were identified using a gas chromatograph (equipped with a PlotQ or an HP5 capillary column) coupled to a mass spectrometer. The mass spectra of most detected reaction products were included in the NIST 08 Mass Spectra Database.

Synchrotron Vacuum Ultraviolet Photoionization Mass Spectrometry Analysis

The main advantage of the two mass spectrometry methods is that the delay between the sampling in the reactor and the analysis using a time-of-flight mass spectrometer is short, enabling the detection of unstable species if their concentration is high enough. The separation of the different isomers is possible thanks the ability to vary the photon energy, but requires much more treatment and the knowledge of the ionization energies. The quantification of a species requires the knowledge of its photoionization cross section which is not available for all species (these data can only be obtained by measuring the response of known amounts of standards when they are available).

Species from the reactor were analyzed online by a reflectron time-of-flight mass spectrometer (RTOF MS) with photo ionization by synchrotron radiation. The reactor was coupled to the low pressure photo ionization chamber through a lateral fused silica cone-like nozzle which was inserted in the spherical part. The tip of the cone was pierced by a 50 μm orifice to obtain a molecular beam. A nickel skimmer with a 1.25 mm diameter aperture was located 15 mm downstream from the sampling nozzle. The sampled gases formed a molecular beam, which was intersected perpendicularly with synchrotron vacuum ultraviolet light. The ion signal was then detected with the RTOF MS, which was installed in the photoionization chamber vertically. Additional details about this experimental apparatus are available in.[28,29]

The relative uncertainty in the mole fractions is ±10% for species directly calibrated using standards (cyclopentene and argon) and ±25% for species calibrated using a reference species and photo ionization cross sections (see(28) for details about the quantification). For species the cross section of which has not been measured, an estimated value was used for the quantification leading to more uncertainty (about a factor of 2).

Single Photon Laser Ionization Mass Spectrometry Analysis

The sampling was performed in the gas phase in the reactor using a deactivated fused silica capillary tube (200 µm inside diameter, 5 m length, flow of 3–4 mL·min^{-1}) heated to 353 K. At the outlet of the heated capillary line, samples were directly injected in the ionization zone of a reflectron time-of-flight mass spectrometer equipped with dual ion source for electron-impact and single-photon ionizations (PhotoTOF, Photonion GmbH, Germany, a custom-device developed for LRGP-Nancy). In the measurements described here, vacuum ultraviolet (VUV) photons with a wavelength of 118 nm (10.6 eV) were used for a single-photon absorption/ionization process. The mass spectrometer covers a mass range of *m/z* 10–2000 with mass resolution of 2000 and mass sensitivity of 100 ppm. Mole-fraction calculations were made using toluene at *m/z* 92 as a reference (using the mole fractions measured by gas chromatography). The relative uncertainty is 25% for products quantified using toluene as a reference and it is larger for species the cross sections of which have been estimated due to a lack of data in the literature (e.g., naphthalene).

Experimental Results

The pyrolysis of cyclopentene was studied in a jet-stirred reactor at a residence time of 1 s, at a pressure of 106.7 kPa (800 Torr) and at temperatures ranging from 773 to 1073 K. The inlet mole fraction of fuel was 0.04. The dilution gas was helium in France and argon in China. Argon was required in China as the signal recorded for m/z 40 is used as a reference for the normalization of signals recorded for other *m/z*. Species were quantified using the three methods described in the previous section: gas chromatography, synchrotron vacuum ultraviolet photoionization mass spectrometry, and single photon ionization mass spectrometry. Table 1 shows the list of quantified species and the method used for the quantification. Some species were quantified with two or three methods, which allowed comparison of the three sets of experiments.

Quantification of species from gas chromatography analysis

Twenty five reaction products were detected in the gas chromatography analyses. These species are hydrogen (H_2) and hydrocarbons. They can be classified as follows:

• Small C_1–C_3 hydrocarbons: methane, acetylene, ethylene, ethane, propene, allene and propyne (Figure 1).

• C_4–C_6 hydrocarbons: 1,3-butadiene, 1- and *iso*-butenes (both species have the same retention time), the two 2-butene isomers, 1,3-cyclopentadiene, the two 1,3-pentadiene isomers, 1,4-pentadiene, 1,5-hexadien-3-yne, and 1,5-hexadiene (Figure 2). In addition three C_6H_8 isomers were detected but could not be identified as they have very close electron impact (70 eV) mass spectra.

• Aromatic species: benzene, toluene, styrene, indene, and naphthalene (Figure 2 and Figure 3).

Identification of Species from SVUV-PIMS Data

Mass spectra were recorded at temperatures ranging from 773 to 1048 K (with a step of 25 K) and at the following photon energies: 9.00, 9.50, 10.00, 10.50, 11.00, 12.30, 14.60, and 16.60 eV.

Identification of species was performed using the photoionization efficiency spectra obtained for the different *m/z*. Figure 4 displays photoionization efficiency spectra for some *m/z* as well as ionization energies (IE) of the corresponding species. Note that a signal was recorded for *m/z* 65 which could be due to the cyclopentadienyl radical and that fulvene was not present in our experiments according to the photoionization efficiency spectrum at *m/z* 78. Ionization energies found in literature are sometimes not accurate (as an example ionization energies of the cyclopentadienyl radical provided by the NIST database[30] are 8.41, 8.56, and 8.7 eV). Zero-point-corrected adiabatic IEs were calculated at the CBS-QB3 level of theory[31] using software Gaussian[32] to compare with literature data (see Supporting Information for details).

Table 1. List of Species Quantified in This Study Using the Three Analytical Methods

Name	Molecular formula	m/z	Ionization energy (eV)[1]	Quantification using gas chromatography	Quantification using SVUV-PIMS	Quantification using SPI-MS
hydrogen	H_2	2	15.43	×	×	
methane	CH_4	16	12.61	×	×	
acetylene	C_2H_2	26	11.40	×	×	
ethylene	C_2H_4	28	10.51	×	×	
ethane	C_2H_6	30	11.52	×		
allene	C_3H_4	40	9.62	×		
propyne	C_3H_4	40	10.36	×		
propene	C_3H_6	42	9.73	×	×	×
1,3-butadiene	C_4H_6	54	9.07	×	×	×
iso- & 1-butene[2]	C_4H_8	56	9.22 & 9.55	×		
2-butene[3]	C_4H_8	56	9.10 (E) & 9.11 (Z)	×		
cyclopentadienyl	C_5H_5	65	8.4 – 8.7		×	×
1,3-cyclopentadiene	C_5H_6	66	8.57	×	×	[4]
1,3-pentadiene[3]	C_5H_8	68	8.59 (E) & 8.62 (Z)	×		
1,4-pentadiene	C_5H_8	68	9.62	×		
cyclopentene	C_5H_8	68	9.01	×	×	[4]
benzene	C_6H_6	78	9.24	×	×	×
1,5-hexadien-3-yne	C_6H_6	78	8.50	×	×	
1,5-hexadiene	C_6H_{10}	82	9.27	×		×
toluene	C_7H_8	92	8.83	×	×	×
styrene	C_8H_8	104	8.46	×	×	×
5-allyl-1,3-cyclopentadiene	C_8H_{10}	106	8.44			×
indene	C_9H_8	116	8.14	×	×	×
naphthalene	$C_{10}H_8$	128	8.14	×	×	×
5-cyclopenta-2,4-diene-cyclopenta-1,3-diene	$C_{10}H_{10}$	130	8.44			×

[1] Ionization energies are literature [30] and calculated values (see Supplemental Data for more information).

[2] The two species have the same retention time and could not be separated in the gas chromatography analysis.

[3] The two Z and E isomers were detected in the gas chromatography analysis.

[4] The species was detected but not quantified because the signal was saturated.

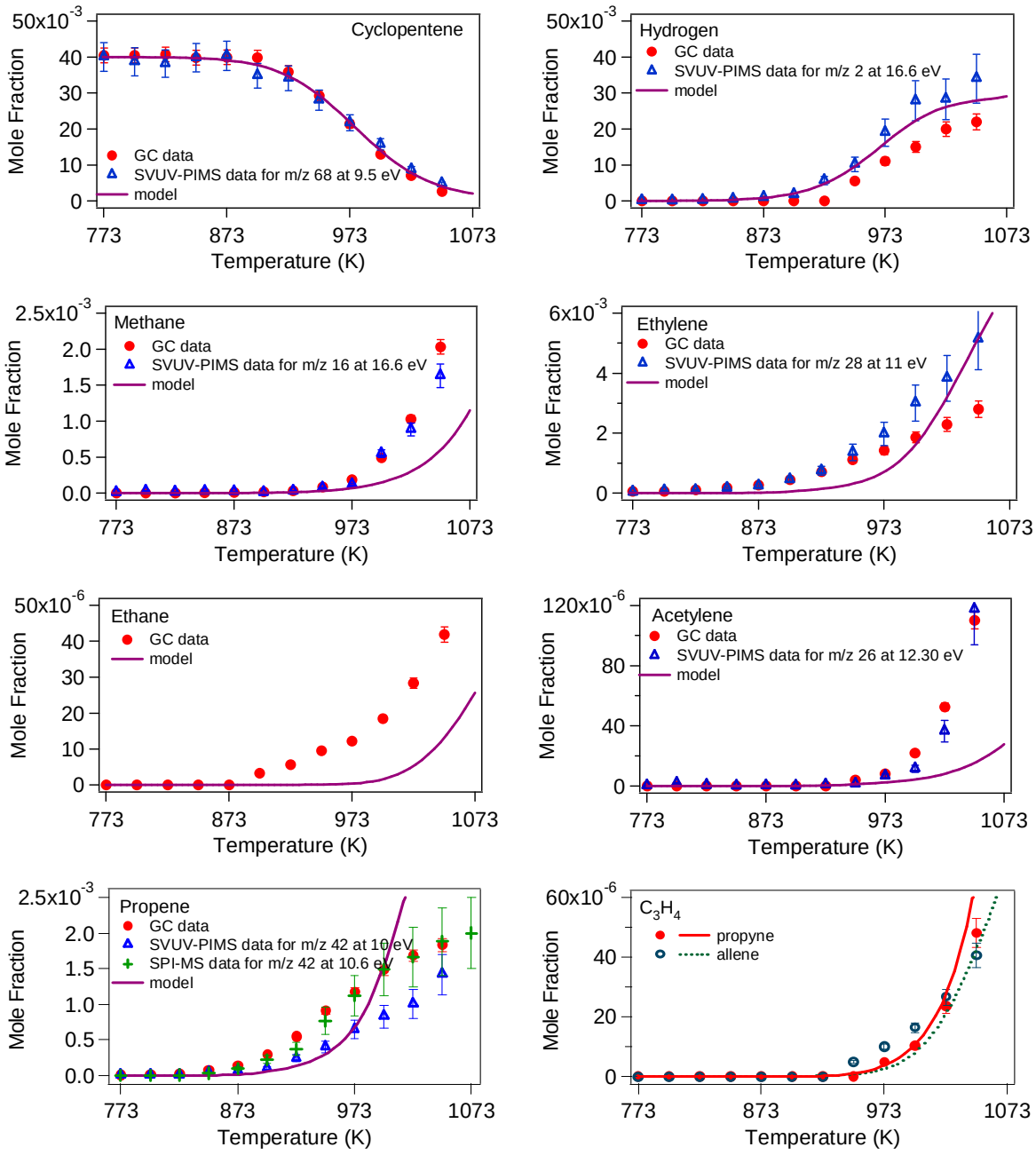

Figure 1. Mole fraction profiles of the reactant (cyclopentene), hydrogen and C_1–C_3 hydrocarbons (● and ○, GC data; △, SVUV-PIMS data; + , SPI-MS).

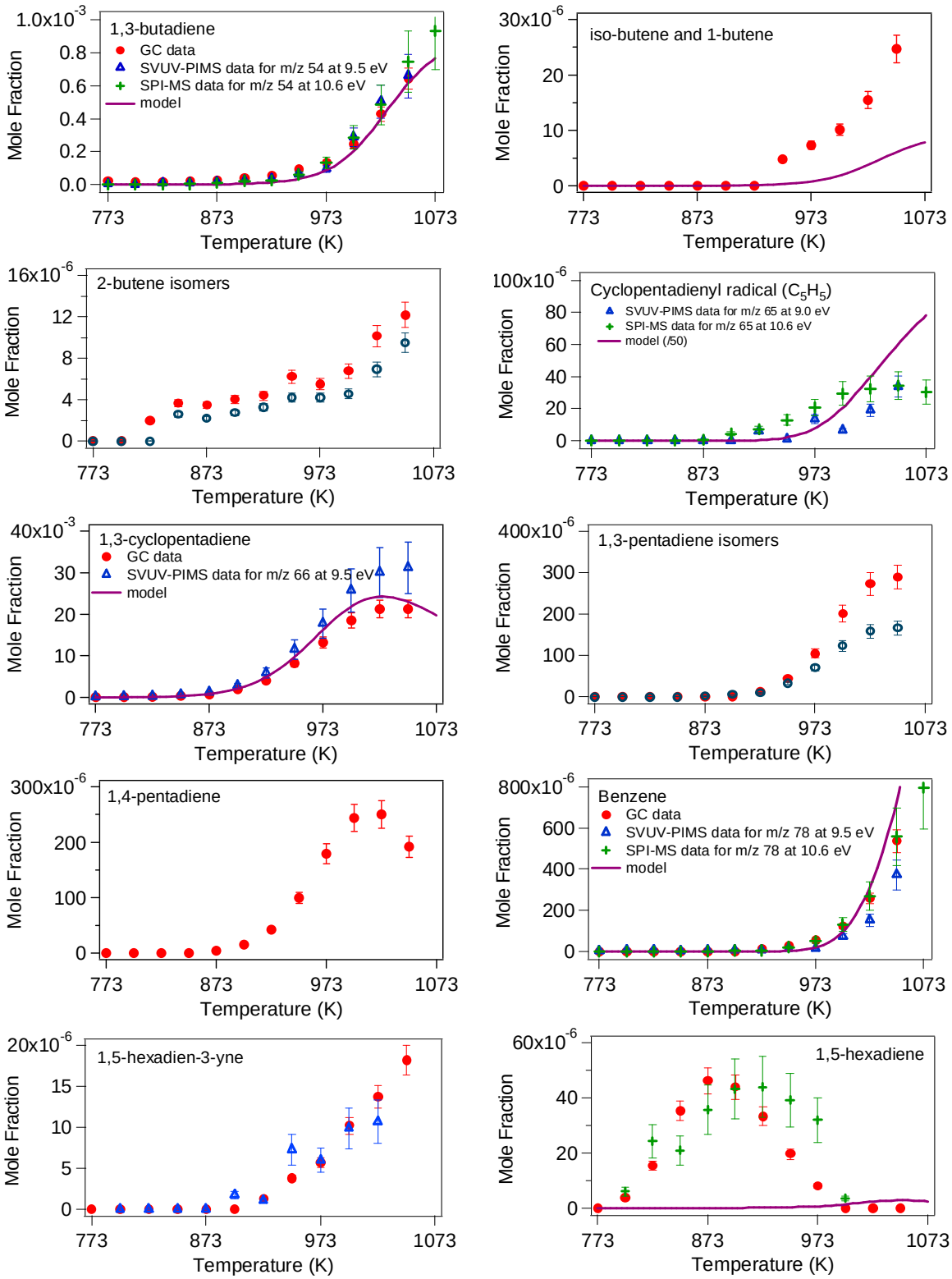

Figure 2. Mole fraction profiles of C_4–C_6 hydrocarbons (● and ○, GC data; △, SVUV-PIMS data; +, SPI-MS data). Mole fractions computed for the cyclopentadienyl radical are divided by a factor of 50.

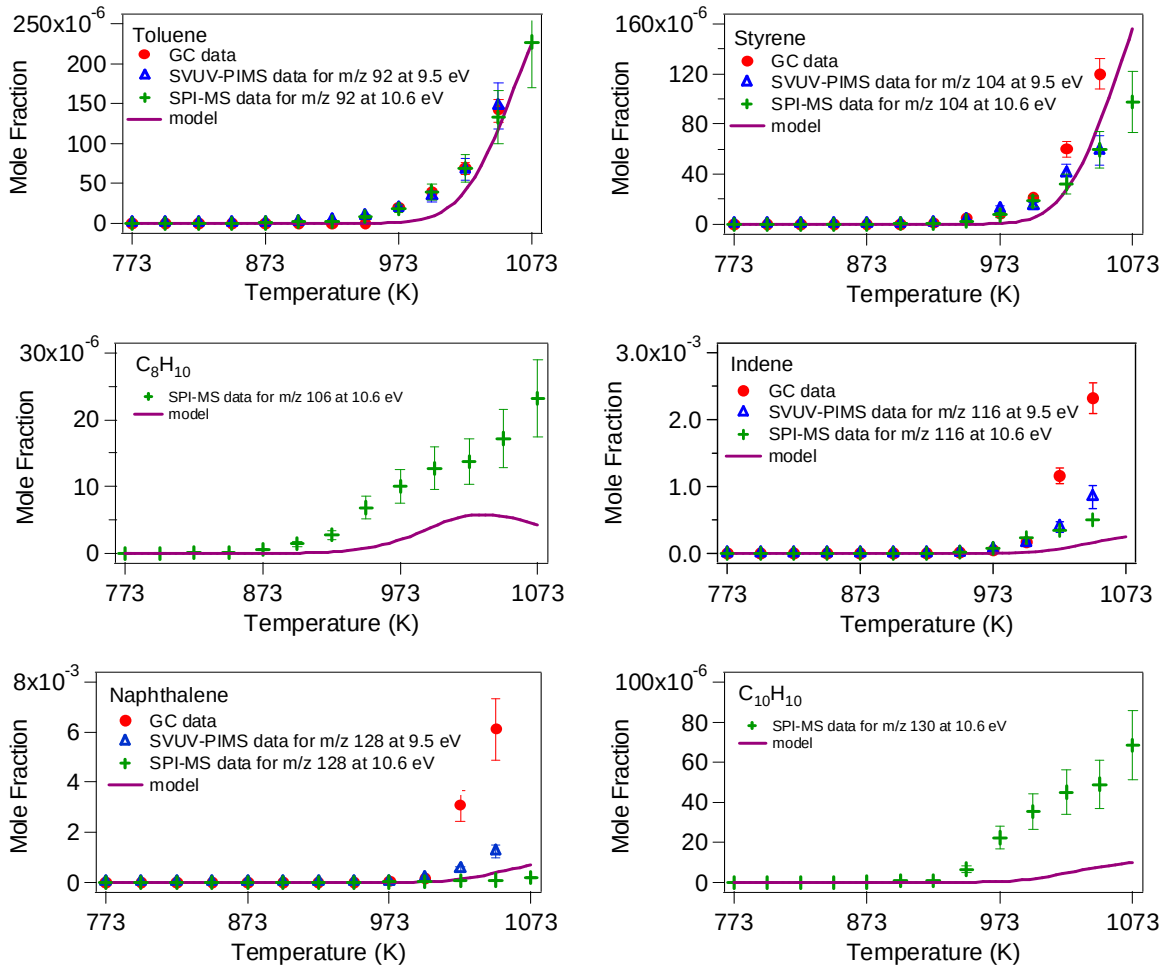

Figure 3. Mole fraction profiles of toluene, styrene, C_8H_{10}, indene, naphthalene, and $C_{10}H_{10}$ (●, GC data; Δ, SVUV-PIMS data; +, SPI-MS data). Note that, except for toluene, styrene and indene, the cross sections used for the quantification are estimated value and may be not accurate.

Species assignment is discussed in detail below for the different *m/z*:

• *m/z* 2: This signal correspond to hydrogen (H_2). Its ionization energy is relatively high (15.43 eV[30]) and the formation of hydrogen could be observed at the highest photon energy (16.6 eV).

• *m/z* 16: The only possible species in our experiments is methane. Its ionization energy is 12.61 eV.[30]

• *m/z* 28: This signal is for ethylene only as carbon monoxide cannot be formed in the pyrolysis of hydrocarbons. It is not for nitrogen given that very pure argon was used as carrier gas. The ionization energy of ethylene is 10.51 eV.[30]

• *m/z* 42: The most probable species is propene which has an ionization energy of 9.73 eV.[30] Note that another candidate for this mass could be cyclopropane which has a ionization energy close to 9.86 eV[30]) but the formation of this species is much less probable than that of propene. The ionization energy of propene (9.73 eV) is in correct agreement with the signal displayed in the photoionization efficiency spectrum of *m/z* 42 (Figure 4).

• *m/z* 65: The signal is weak. It could correspond to the cyclopentadienyl radical (C_5H_5) or to a fragment coming from a larger ion (such as $C_5H_6^+$). According to the literature,[10,33-35] the ionization energy of the cyclopentadienyl radical is lying in between 8.41 and 8.7 ± 0.1 eV. The ionization energy calculated using Gaussian[32] is 8.73 eV (see Supporting Information for details about calculations). This last value is

consistent with the increase of the signal at *m/z* 65 which is observed in the photoionization efficiency spectrum shown in Figure 4. The assignment may not be accurate as the signal for this *m/z* is weak. Nevertheless the quantification of this radical was performed (see section thereafter). Note that, to our knowledge, apart in the case of OH and HO_2 using optical method,[36] radicals have never been detected during JSR experiments.

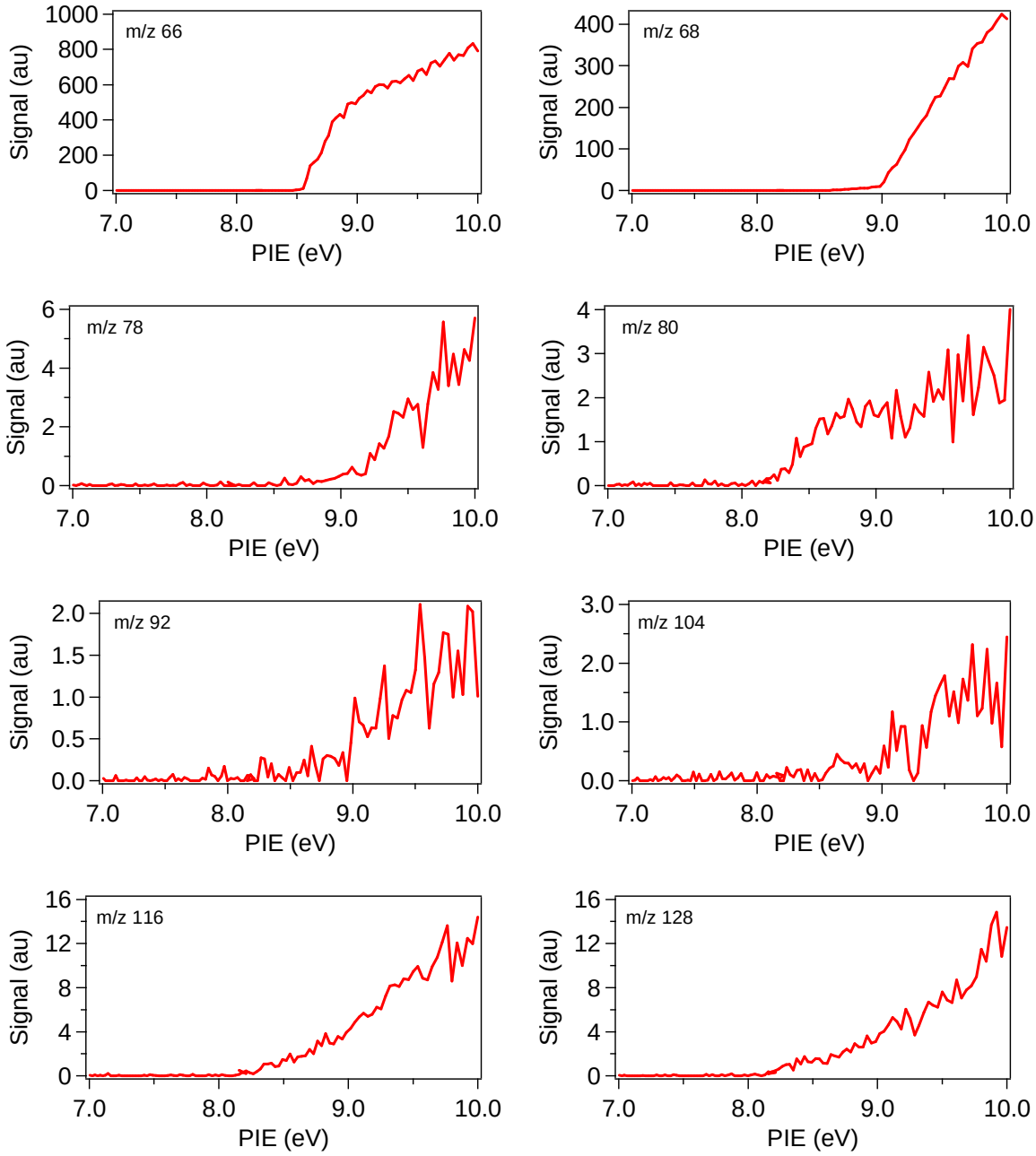

Figure 4. Photoionization efficiency spectra of several *m/z* sampled from the reactor (the reaction temperature was 998 K).

• *m/z* 66: The signal is for 1,3-cyclopentadiene. Its ionization energy is 8.57 eV.[30] This is consistent with the data displayed in photoionization efficiency spectrum of *m/z* 66 (Figure 4).
• *m/z* 68: The signal corresponds to the reactant (cyclopentene) and other C_5H_8 species such as 1,3-pentadiene and 1,4-pentadiene. Ionization energies are 8.59, 8.92, and 9.01 eV for 1,3-pentadiene, cyclopentene and 1,4-pentadiene, respectively.[30] The ionization energy of 1,3-pentadiene (8.59 eV) well corresponds to the photoionization energy at which the signal starts increasing from zero in the photoionization efficiency spectrum of *m/z* 68 (Figure 4). An abrupt change in the slope of the curve is observed around 9.00 eV due to the ionization of cyclopentene (IE of 9.01 eV). Note that contributions of 1,3- and 1,4-pentadienes are masked by the one of the reactant above this photon energy.
• *m/z* 78: There are several possible isomers. The signal starts increasing from about 8.50 eV which corresponds to 1,5-hexadien-3-yne (IE of 8.50 eV[30]). The change in the slope which is observed around 9.20 eV is due to the detection of benzene (IE of 9.24 eV[30]). Fulvene was not detected in this study as its ionization energy is lower than 8.50 eV (it is 8.36 eV[30]). Note that the identification of 1,5-hexadien-3-yne is quite certain as other possible linear C6H6 isomers have higher ionization energies.
• *m/z* 80: This signal can correspond to many C6H8 isomers making the species assignment very uncertain. Possible C6H8 isomers could be 1,3-cyclohexadiene (IE of 8.25 eV[30]), 1,4-cyclohexadiene (IE of 8.82 eV[30]), and 5-methyl-1,3-cyclopentadiene (IE of 8.45 eV[37]). But other methylcyclopentadiene isomers and linear unsaturated C_6H_8 isomers cannot be excluded. The signal starts increasing at about 8.1 eV in the photoionization efficiency spectrum of *m/z* 80 (Figure 4) and there is a change in the slope at about 8.45 eV possibly due to 5-methyl-1,3-cyclopentadiene.
• *m/z* 92: This is the signal for toluene. Its ionization energy is 8.83 eV. [30] The signal starts increasing below this energy. This is likely due to the detection of a fragment coming from the decomposition of a larger ion (note that indene and naphthalene have lower ionization energies).
• *m/z* 104: This is the signal for styrene which has an ionization energy of 8.46 eV. [30] This value is consistent with the photoionization efficiency spectrum recorded for *m/z* 104.
• *m/z* 116: This is the signal for indene. Its ionization energy (8.14 eV[30]) is in good agreement with the photoionization efficiency spectrum of *m/z* 116 (Figure 4).
• *m/z* 128: This is the signal for naphthalene which has an ionization energy of 8.14 eV.[30] Again the ionization energy of this species corresponds well with the photon energy at which the signal starts increasing in the photoionization efficiency spectrum of *m/z* 128 (Figure 4).

Quantification of Species from SVUV-PIMS Data

Mole fraction of species detected using SVUV-PIMS were determined and compared with mole fractions obtained from gas chromatography analyses. Some species could not be quantified because of a lack of data concerning cross sections. There is also a lack of precision in the cross section of some species (such as naphthalene) making SVUV-PIMS mole fractions less accurate than those obtained using gas chromatography.

The reactant was calibrated by measuring the signal for m/z 68 under unreactive conditions. Mole fractions of reaction products were calculated using the signal of the reactant or that of argon as a reference using equation 1.

$$x_i(T) = x_{ref}(T) \times \frac{S_i(T)}{S_{ref}(T)} \times \frac{\sigma_{ref}(E)}{\sigma_i(E)} \times \frac{D_{ref}}{D_i} \quad (1)$$

$x_i(T)$ and $S_i(T)$ are the mole fraction and the signal of a species i at temperature T, respectively. $\sigma_i(E)$ is the photoionization cross-section of the species i at the photon energy E. D_i is the mass discrimination factor of species i.

Hydrogen (H_2) was quantified using the signal for *m/z* 2 and the one of argon (*m/z* 40) as a reference at 16.60 eV. Cross sections used for the quantification were 9.72 and 32.14 Mb for hydrogen and argon, respectively.[38,39] Methane mole fractions were also determined using the signal of argon as a reference. Calculations were performed using signals for *m/z* 16 and *m/z* 40 at 16.60 eV. The cross section of methane is 44.38 Mb at this photon energy.[40] Acetylene mole fractions were calculated from the signal detected for *m/z* 26 at 12.30 eV and using ethylene as reference. Cross sections of acetylene and ethylene are 29.7 and 4.6 Mb, respectively, at 12.30 eV.[41,42]

Other species have lower ionization energies and were quantified using the signal of the reactant (*m/z* 68) as a reference. Ethylene mole fractions were calculated using the two signals at *m/z* 28 and 68 at 11.00 eV. Cross sections were 7.759 and 14.22 Mb for ethylene and cyclopentene, respectively, at this ionization energy.[42] Propene was quantified using the signals for *m/z* 42 and 68 at 10.00 eV. Cross sections were 7.05 and 11.15 Mb for propene and cyclopentene, respectively, at this ionization energy.[42,43]

1,3-Butadiene, 1,3-cyclopentadiene, benzene, toluene, styrene, indene, and naphthalene were quantified using the signal for *m/z* 68 at 9.50 eV as a reference (the cross section of cyclopentene is 6.18 Mb at this photon energy[42]). Cross sections used for the quantification were 10.33,[42] 15.67,[10] 11.05,[42] 18.54,[44] 26.33,[44] 27.61, [44] and 20.26 Mb for 1,3-butadiene, 1,3-cyclopentadiene, benzene, toluene, styrene, indene, and naphthalene, respectively, at 9.50 eV. The cross section of naphthalene used in the present work (20.26 Mb) was estimated using the method of group additivity proposed by Bobeldijk et al.[45] as no accurate measurement were found in the literature. The cross section of 1,3-cyclopentadiene at 9.5 eV proposed by Hansen et al. (15.67 Mb)[10] is different from the value proposed by Taatjes et al. (10.05 Mb).[46] The value proposed by Hansen et al.[10] was used in the present work.

The quantification of the cyclopentadienyl radical (*m/z* 65) was performed using the signal at *m/z* 66 (1,3-cyclopentadiene) at 9.00 eV as a reference. Cross sections are 3.78 and 11.65 Mb for the cyclopentadienyl radical and 1,3-cyclopentadiene, respectively, at 9.00 eV.[10] The mole fraction profile of the cyclopentadienyl radical is displayed in Figure 2. A maximum mole fraction of 34 ppm is obtained at 1048 K for this species. This is 1000 times less than the mole fraction of 1,3-cyclopentadiene in the same conditions. Mole fractions of 1,5-hexadien-3-yne were calculated using the same procedure as the cyclopentadienyl radical at 9.00 eV (a photon energy less than the ionization energy of benzene) with a cross section of 22.72 Mb estimated using the method of group additivity proposed by Bobeldijk et al.[45] A factor of 165 was obtained between benzene and 1,5-hexadien-3-yne mole fractions at 1023 K meaning that the contribution of 1,5-hexadien-3-yne to the signal at *m/z* 78 is negligible compared to that of benzene at 9.50 eV (the photon energy at which benzene was quantified).

Species Detection Using SPI-MS

Figure 5 displays a typical mass spectrum recorded during the pyrolysis of cyclopentene at 1073 K. The peaks detected using this technique provided useful information. They confirmed the observations made using SVUV-PIMS as the same peaks were detected: *m/z* 42 (propene), 54 (1,3-butadiene), 65 (cyclopentadienyl radical), 66 (1,3-cyclopentadiene), 68 (cyclopentene), 78 (benzene and 1,5-hexadien-3-yne), 80 (C_6H_8 isomers), 92 (toluene), 104 (styrene), 116 (indene), and 128 (naphthalene). A peak at m/z 82 (1,5-hexadiene) was also detected but is not visible in the spectrum in Figure 5 due to a low concentration at 1073 K.

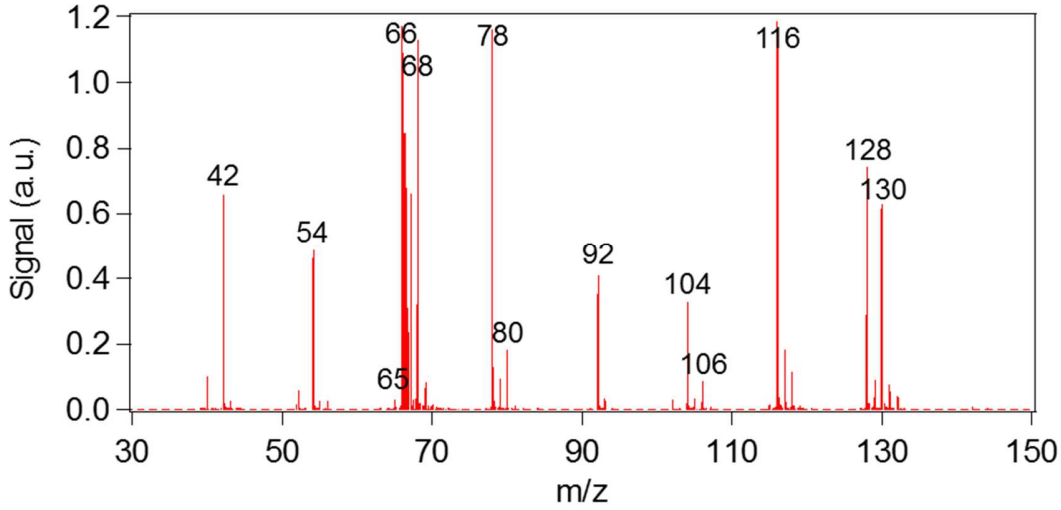

Figure 5. Mass spectrum obtained during the pyrolysis of cyclopentene (1073 K) using SPI-MS.

These analyses enabled the detection of two new peaks at m/z 106 and 130. They could not be detected using SVUV-PIMS likely because amounts were below the detection limit. The m/z of these two peaks correspond to those of C_8H_{10} and $C_{10}H_{10}$ species. As these species could not be detected using SVUV-PIMS, photoionization efficiency spectra could not be recorded making the identification impossible. But the large quantities of propene and 1,3-cyclopentadiene detected in experiments suggest that concentrations of allyl and cyclopentadienyl radicals are likely important and that their reactions of combination could lead to C_8H_{10} and $C_{10}H_{10}$ termination products, similarly to 1,5-hexadiene (the combination product from two allyl radicals) which was detected using gas chromatography and SPI-MS. Figure 6 displays the probable structures of the two recombination products: 5-allyl-1,3-cyclopentadiene (C_8H_{10}) obtained from the combination of allyl and cyclopentadienyl radicals; 5-cyclopenta-2,4-diene-cyclopenta-1,3-diene ($C_{10}H_{10}$) from the combination of two cyclopentadienyl radicals. The ionization energies of these two species, calculated using Gaussian,[32] were 8.44 eV for each, which is below the photon energy of 10.6 eV used in experiments.

5-allyl-1,3-cyclopentadiene 5-cyclopenta-2,4-diene-cyclopenta-1,3-diene

Figure 6. Probable structures of C_8H_{10} and $C_{10}H_{10}$ species detected using SPI-MS.

The quantification performed using SPI-MS data allowed to compare mole fractions with those obtained using the two other techniques (GC and SVUV-PIMS). The same procedure as for SVUV-PIMS data was used. But unlike SVUV-PIMS experiments, the carrier gas and the fuel could not be used as references. The photon energy (10.6 eV) was too low to ionize the carrier gas and the fuel signal at *m/z* 68 was saturated. Toluene (*m/z* 92) mole fractions obtained using GC were chosen as a reference for the quantification of other species: propene, 1,3-butadiene, the cyclopentadienyl radical, benzene, 1,5-hexadiene, styrene, indene, naphthalene and the two C_8H_{10} and $C_{10}H_{10}$ species which are supposed to be combination products. Note that the signal at *m/z* 78 (benzene and 1,5-hexadien-3-yne) was attributed to benzene for

the quantification as the contribution of 1,5-hexadien-3-yne is extremely low (almost 2 orders of magnitude between the mole fractions of the two species according to GC and SVUV-PIMS data).

Cross sections at 10.6 eV used for the quantification have the same origins as those used for the treatment of SVUV-PIMS data when found in the literature (see previous section for references). When no data were available (e.g., for naphthalene and the two C_8H_{10} and $C_{10}H_{10}$ combination products), they were estimated using the method of group additivity proposed by Bobeldijk et al.[45] Mole fractions profiles obtained using SPI-MS data are displayed in Figure 1 to Figure 3.

Atom balances

Carbon and hydrogen atom balances have been calculated for each experiment over the whole range of studied temperatures (see Supporting Information). The expression used for the calculation of the balance of an atom i is given by equation 2.

$$balance = \frac{\sum_j \left(n_i^j \times x_j^{outlet} \right)}{n_i^{fuel} \times x_{fuel}^{inlet}} \qquad (2)$$

where n_i^j is the number of atom i in the species j, x_j^{outlet} is the mole fraction of the species j at the outlet of the reactor, n_i^{fuel} is the number of atom i in the fuel, and x_{fuel}^{inlet} is the mole fraction of the fuel at the inlet of the reactor.

Both carbon and hydrogen atom balances are around 100%. For carbon atom, it is 100 ± 6%, and for hydrogen, it is 98 ± 6%.

Modeling

The model of the thermal decomposition of cyclopentene is based on a previous model for the oxidation of ethylbenzene.[22] This model contains a comprehensive C_0–C_2 reaction base, a reaction base for the reactions of C_3–C_5 unsaturated hydrocarbons (like allene, propyne, 1,3-butadiene, cyclopentene, and 1,3-cyclopentadiene), and the chemistry of the formation of small aromatics (benzene and toluene).
This model was first tested without any changes. A good agreement was obtained for the fuel conversion and primary products like 1,3-cyclopentadiene, propene and ethylene, whereas mole fractions of aromatics were strongly underestimated (except for naphthalene but the formation route included in the model was a rough assumption which was removed afterward and replaced by a new chemistry set based on the theoretical study by Kislov and Mebel[17]).

Kinetic parameters of the main reactions involving the fuel and radicals deriving from the fuel (cyclopentene) are given in Table 2. Reactions taken into account are the unimolecular decomposition to 1,3-cyclopentadiene and hydrogen (this reaction is very important under pyrolysis conditions), unimolecular initiations by breaking of C–H bonds to the cyclopent-3-en-1-yl radical and the allylic cyclopent-2-en-1-yl radical, H atom abstractions also forming these two radicals, and the addition of H atom to the double bond leading to the cyclopentyl radical. Only the main reactions of decomposition of radicals are given in Table 2.

Table 2. Rate Parameters of Main Reactions Involved in the Primary Mechanisms (Units: cm^3, mol, s, cal), with $k = A \times T^n \times exp(-E_a/RT)$

Reaction	A	n	Ea	Reference
Molecular decomposition				
cyclopentene ⇆ C_5H_6# + H_2	2.24×10^{13}	0	60.01×10^3	[54]
Unimolecular initiations (written in reverse way)				
C_5H_7#[a] + H ⇆ cyclopentene	1.00×10^{14}	0	0	[55]
C_5H_7#Y[b] + H ⇆ cyclopentene	1.00×10^{14}	0	0	[55]
H-atom abstractions				
cyclopentene + H ⇆ C_5H_7# + H_2	9.00×10^6	2.00	5.00×10^3	[55]
cyclopentene + H ⇆ C_5H_7#Y + H_2	1.08×10^5	2.50	9.79×10^3	[56]
cyclopentene + CH_3 ⇆ C_5H_7# + CH_4	2.00×10^{11}	0	9.60×10^3	[55]
cyclopentene + CH_3 ⇆ C_5H_7#Y + CH_4	2.00×10^{11}	0	7.30×10^3	[56]
cyclopentene + C_2H_5 ⇆ C_5H_7# + C_2H_6	2.00×10^{11}	0	11.00×10^3	[56]
cyclopentene + C_2H_5 ⇆ C_5H_7#Y + C_2H_6	8.80	3.5	4.14×10^3	[56]
cyclopentene + C_3H_5Y ⇆ C_5H_7# + C_3H_6	3.20×10^{12}	0	15.10×10^3	[9]
cyclopentene + C_3H_5Y ⇆ C_5H_7#Y + C_3H_6	4.00×10^1	3.30	18.17×10^3	[9]
Additions to cyclopentene (written in the reverse way)				
C_5H_9#[c] ⇆ cyclopentene + H	4.79×10^{12}	0.57	34.43×10^3	[57]
Decompositions of radicals				
C_5H_7# ⇆ 1,3-cyclopentadiene + H	6.40×10^{13}	0	34.80×10^3	[56]
C_5H_7#Y ⇆ 1,3-cyclopentadiene + H	3.00×10^{13}	0	50.50×10^3	[56]
C_5H_9# ⇆ C_5H_9[d]	2.95×10^{12}	0.847	35.42×10^3	[57]
C_5H_9 ⇆ ethylene + C_3H_5Y	9.12×10^{11}	0.39	24.59×10^3	[58]
C_5H_9 ⇆ C_5H_9Y[e]	3.80×10^{11}	0.67	30.60×10^3	[f]
C_5H_9Y ⇆ 1,3-butadiene + CH_3	5.75×10^{13}	0.10	35.90×10^3	[58]

[a] C_5H_7# is the cyclopent-3-en-1-yl radical.

[b] C_5H_7#Y is the allylic cyclopent-2-en-1-yl radical.

[c] C_5H_9# is the cyclopentyl radical.

[d] C_5H_9 is the pent-4-en-1-yl radical.

[e] C_5H_9Y is the allylic 1-Penten-3-yl radical.

[f] estimated from the reaction of isomerization of pent-1-yl radical to pent-4-yl radical[59] with a correction of -6 kcal mol^{-1} to Ea to take into account the allylic nature of the shifted H-atom.

Reactions have been added to this model to better account for the formation of aromatics and naphthalene. This was done by taking into account reactions of the cyclopentadienyl radical which plays a very important role in the pyrolysis of cyclopentene. Indeed large amounts of this radical are obtained from 1,3-cyclopentadiene which is the main product from the decomposition of cyclopentene. Reactions displayed in Figure 7 have been included in the model to explain the formation of benzene from cyclopentadienyl radicals. The first step (reaction 1 in Figure 7) is the termination by combination of cyclopentadienyl and methyl radicals forming 5-methyl-1,3-cyclopentadiene (note that this species was likely among the C_6H_8 isomers detected in experiments but it could not be identified with certainty). Then this molecule leads to two radicals, one of them being resonantly stabilized, by H atom abstractions and unimolecular initiation by C–H bond breaking (steps 2a and 2b in Figure 7). Reactions of the resonantly stabilized radical are limited: it can isomerize to the other nonresonantly stabilized radical (step 3), or decompose to fulvene (not shown in Figure 7). Reaction 4 is an intra addition on a double bond forming a bicyclic radical which can react by a β-scission (step 5) to yield the cyclohexadienyl radical. This radical can then decompose to benzene by C–H β-scission (reaction 6). This pathway involving a bicyclic radical was proposed by Lifshitz et al.[47] in their study of decomposition and ring extension in 5-methyl-1,3-cyclopentadiene. This pathways has a relatively low activation energy (17.4 kcal.mol^{-1}).[14] This sequence of reactions via bicyclic radicals was also used by Mulholland et al.[11] and McGivern et al.[48] to explain the growth of polycyclic aromatic hydrocarbon during the pyrolysis of 1,3-cyclopentadiene.

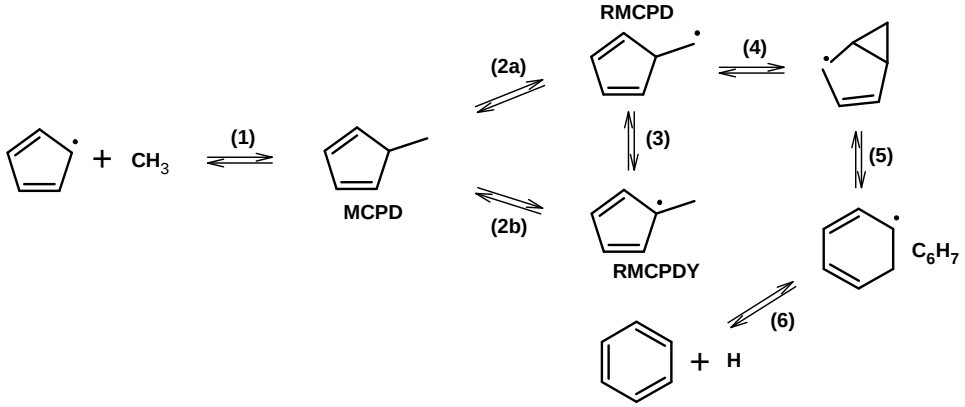

Figure 7. Reactions added in the model to account for the formation of benzene from the cyclopentadienyl radical.

Note that the radical formed by step 2a can also react by a C–C β-scission yielding a linear radical which can react by an intra addition to a double bond to give the cyclohexadienyl radical (not shown in Figure 7). This sequence of reaction was also added in the model but simulations showed that it was not competitive with the bicyclic radical pathway in the conditions of our study due to the higher activation energy of the C–C β-scission (35 kcal.mol^{-1}). The kinetic parameters of the reactions shown in the scheme in Figure 7 are given in Table 3.

Table 3. Kinetic Parameters Used for the Formation of Benzene from the Cyclopentadienyl Radical As Shown in Figure 5 (Units: cm^3, mol, s, cal), with $k = A \times T^n \times exp(-E_a/RT)$

Reaction	A	n	Ea	Reference
Combination				
$C_5H_5 + CH_3 \leftrightarrows$ MCPD[a]	8.34×10^{15}	-0.70	-0.50	[60]
Unimolecular initiation				
RMCPD[b] + H ⇆ MCPD	1.0×10^{14}	0	0	[9]
MCPD ⇆ RMCPDY[c] + H	2.5×10^{15}	0	78.7×10^3	as for $C_5H_6 \leftrightarrows C_5H_5$ + H with A/2 [61]
H-atom abstraction				
MCPD + H ⇆ RMCPD + H_2	2.9×10^7	2.0	7.7×10^3	[55]
MCPD + H ⇆ RMCPDY + H_2	1.7×10^5	2.5	2.48×10^3	as for propene + H ⇆ C_3H_5Y + H_2 [62]
MCPD + CH_3 ⇆ RMCPD + CH_4	0.75×10^{-7}	6.0	5.8×10^3	as $C_2H_6 + CH_3 \leftrightarrows C_2H_5 + CH_4$ and A/2 [63]
MCPD + CH_3 ⇆ RMCPDY + CH_4	0.9×10^{-1}	4.0	0	as $C_5H_6 + CH_3 \leftrightarrows C_5H_5 + CH_4$ and A/2 [64]
MCPD + C_3H_5Y ⇆ RMCPD + C_3H_6	4.0×10^1	3.3	19.84×10^3	[9]
MCPD + C_3H_5Y ⇆ RMCPDY + C_3H_6	0.8×10^{12}	0	15.1×10^3	[9]
MCPD + C_5H_5 ⇆ RMCPD + C_5H_6	8.0×10^1	3.3	19.84×10^3	[9]
MCPD + C_5H_5 ⇆ RMCPDY + C_5H_6	1.6×10^{12}	0	15.1×10^3	[9]
Isomerization				
RMCPDY ⇆ RMCPD	3.0×10^{12}	0	50.4×10^3	[14]
Reactions of decomposition to benzene [d]				
RMCPD ⇆ C_6H_7 [e]	1.4×10^{13}	0	17.4×10^3	[14]
benzene + H ⇆ C_6H_7	3.2×10^{13}	0	3.2×10^3	[65]

[a] MCPD is the 5-methyl-1,3-cyclopentadiene

[b] RMCPD is the 5-methylene-1,3-cyclopentadiene radical.

[c] RMCPDY is the resonantly stabilized methyl-cyclopentadienyl radical.

[d] The two reactions (4) and (5) in Figure 3 are globalized in the detailed kinetic model as suggested by Dubnikova and Lifshitz.[14]

[e] C_6H_7 is the cyclohexadi-1,3-en-5-yl radical.

Following the same scheme as in Figure 7, similar reactions have been added for the formation of:
- toluene (from the combination of cyclopentadienyl and ethyl radicals);
- styrene (from the combination of cyclopentadienyl and allyl radicals);
- and naphthalene (from the combination of two cyclopentadienyl radicals).

Schemes representing the formation of toluene and styrene from the cyclopentadienyl radicals are given in Supporting Information (Figures S1 and S3) as well as associated kinetic parameters (Tables S2 and S4). Note that simulations performed with the model showed that the route from cyclopentadienyl and ethyl

radicals to toluene did not play a role under the present conditions because the concentration of ethyl radicals was very low. Thus, another route was considered by considering the addition of the cyclopentadienyl radical to propene (which is abundant). To our knowledge, there is no theoretical study about this system in literature. Thus, the scheme used in the present model was inspired from the theoretical study of the reaction of acetylene and the cyclopentadienyl radical by Fascella et al.[15] The reaction path diagram considered in the present model in shown in Figure S3 and associated kinetic parameters are given in Table S3. Note that the kinetic parameters of the first step (addition of the cyclopentadienyl radical to propene) are very sensitive under the conditions of the present study. There is no data in literature for this reaction and theoretical calculations would be valuable for improving the chemistry data involved in this pathway.

The reactions added for the formation of naphthalene (Figure 8) replace the reaction of combination of two cyclopentadienyl radicals forming naphthalene and two H atoms with an activation energy equal to zero that was present in the first version of the model. The production of naphthalene was also considered through a similar scheme as for benzene, toluene, and styrene, starting with the combination of two cyclopentadienyl radicals yielding the 9,10-dihydrofulvalene. A submechanism was written for the consumption of 9,10-dihydrofulvalene to naphthalene. Unimolecular initiations by breaking of a C–H bond and H atom abstraction leading to the 9-H-fulvalenyl radical have been considered. The fate of this radical is considered through a set of reactions proposed by Kislov and Mebel.[17] They proposed several routes from the 9-H-fulvalenyl radical to naphthalene, azulene, and fulvalene. According to rate parameters, only the so-called spiran pathway to naphthalene was expected to play a role under the temperature conditions of the present study, but simulations showed that fulvalene is also formed in non-negligible amount. These authors also proposed direct routes to naphthalene starting from the 9,10-dihydrofulvalene molecule.[18] Given the large energies obtained from their theoretical calculations, these pathways do not play a role here. Kinetic parameters used in the model were derived from the fitting of their rate constant values between 300 and 1500 K (see Table S5).

Several routes were tested for the formation of indene. The first route which was considered was the addition of the benzyl radical to acetylene. But this path does not play a role here given the low concentrations of benzyl radicals. A second route was tested by considering the reaction of the phenyl radical with 1,3-butadiene and propene (with the chemistry proposed by Fascella et al.[49] and by Kislov and Mebel,[50] respectively). Again this pathway is unimportant because of the low concentration of phenyl radicals. The third route, which was proposed by Fascella et al.,[15] consisted in sequences of reactions starting with the addition of the cyclopentadienyl radical to acetylene (Figure S5). Simulations showed that these sequences of reactions do not account for the formation of indene. Note that a pathway with two successive additions to acetylene ($C_5H_5 + C_2H_2 \rightleftarrows C_7H_7$, $C_7H_7 + C_2H_2 \rightleftarrows C_9H_9$, $C_9H_9 \rightleftarrows \cdots$) was also tested. As for the other sequences of reactions, this third pathway is not important because concentrations of radicals obtained through the first addition to acetylene are low. The last route which was considered was the addition of the cyclopentadienyl radical to 1,3-butadiene, followed by a cyclization, an H-shift, a C–H β-scission and a loss of H_2 to form the aromatic ring (see Figure S6 and Table S6 in Supporting Information). The reaction of addition of the cyclopentadienyl radical to 1,3-butadiene is sensitive for indene formation. To our knowledge there is no value for the kinetic parameters of this reaction in the literature. The value used in the model is that of the reaction of addition of the cyclopentadienyl radical to 1,3-cyclopentadiene proposed by Kislov and Mebel.[51]

Discussion

The comparison of mole fractions measured using the different analytical techniques is discussed as well as probable reasons for discrepancies. Then the abilities of the detailed kinetic model developed in this work to represent the experimental data are presented. A kinetic analysis was then performed to highlight the specificities of the thermal decomposition of cyclopentene as well as the routes to aromatic and poly aromatic species.

Comparison of Mole Fraction Profiles Obtained with the Three Analytical Techniques

The overall agreement between the three sets of experimental data is satisfactory (see Figures 1–3). There is a very good agreement for fuel mole fractions obtained by GC and SVUV-PIMS (Figure 1). Note that the fuel could not be quantified using SPI-MS because the signal was saturated. A very good agreement was also obtained for 1,3-butadiene, benzene (Figure 2) and toluene (Figure 3) which were quantified using the three analytical methods. GC and SVUV-PIMS mole fractions of 1,5-hexadien-3-yne compare very well although the cross section was estimated due to literature data scarcity. The comparison with SPI-MS data could not be performed as the signal contribution of this species was masked by that of benzene.

As far as nonaromatic hydrocarbons are concerned, a good agreement between GC and SVUV-PIMS data is obtained for methane and acetylene (Figure 1). Discrepancies are observed for hydrogen, ethylene and 1,3-cyclopentadiene: SVUV-PIMS mole fractions are larger than GC ones by a factor of 1.5 at 1048 K. The larger SVUV-PIMS mole fractions are likely due to the contribution of fragments from larger ions. Discrepancies between GC and SVUV-PIMS mole fractions for propene cannot be explained by the contribution of fragments from larger ions as SVUV-PIMS mole fractions are lower than GC and SPI-MS ones which compare well. But the literature shows that there are discrepancies in cross sections of propene around 10 eV (the photon energy used for the SVUV-PIMS quantification) whereas the literature agreement is better around 10.6 eV.[43,52,53]

Mole fractions obtained by SPI-MS and SVUV-PIMS for the cyclopentadienyl radical are similar. The shapes of the two mole fraction profiles seem to be different but the SVUV-PIMS mole fraction profiles were calculated from very low signals close to the detection limit. Discrepancies are visible for GC and SPI-MS data for 1,5-hexadiene in the range 900–1000 K: SPI-MS mole fractions are larger (up to a factor of 3) than GC ones. There is no obvious explanation for these discrepancies, but note that 1,5-hexadiene mole fractions are very low.

As far as aromatic compounds larger than toluene are concerned (styrene, indene and naphthalene), discrepancies are observed between the three sets of mole fractions. GC mole fractions are larger than SVUV-PIMS and SPI-MS ones. The difference between mole fractions seems to increase with the size of the compounds: they are more important for naphthalene than for indene and styrene. For these species, the reasons for the discrepancies is likely their lower volatility as well as the sampling method. For the GC analyses, the heated transfer line was a cooper tube (4.83 mm inside diameter) with a longer residence time (by a factor of about 5) than in a capillary tube toward the mass spectrometer, and the injection of gas samples was performed thanks to a loop mounted on a six-way valve. The experimental data obtained in this study suggest that the method used for the sampling of large species is crucial for the reliability of results and the sampling using a capillary tube or a molecular beam is recommended given the better agreement between SVUV-PIMS and SPI-MS data.

Comparison of Computed and Experimental Data

Simulations with the new model lead to an agreement which is overall satisfactory for the fuel conversion and the mole fraction profiles of main reaction products like hydrogen (Figure 1) and 1,3-cyclopentadiene (Figure 2). Mole fractions of benzene (Figure 2), toluene and styrene (Figure 3) are better reproduced by the model with the inclusion of the new formation pathways. But there are still discrepancies for indene and naphthalene (Figure 3) whose computed mole fractions are underpredicted (with a larger deviation for indene). Computed mole fractions of the cyclopentadienyl radical are overpredicted of about a factor 100 (Figure 2). This can be due to the loss of this very reactive species during the sampling or to uncertainties in the chemistry used in the model. No comparison could be done for 1,5-hexadien-3-yne as this species is not included in the model. No attempt was made to include reactions to account for its formation as there is no data in literature concerning its chemistry. Discrepancies are also observed for combination products: 1,5-hexadiene, 5-allyl-1,3-cyclopentadiene, and 5-cyclopenta-2,4-diene-cyclopenta-1,3-diene. Computed mole fractions of these species are underpredicted by the model. The underprediction for 5-allyl-1,3-cyclopentadiene, and 5-cyclopenta-2,4-diene-cyclopenta-1,3-diene is by factors of 2 and 3, respectively. For 1,5-hexadiene, data computed using the model are underpredicted and the shape of the mole fraction profiles is not well predicted. For this species, the peak mole fraction visible in Figure 2 is located around 900 K, which is a relatively low temperature for which the fuel conversion is low. The underprediction of 1,5-hexadiene mole fraction suggests that formation routes to allyl radical or more direct ones to 1,5-hexadiene are underestimated by the model below 1000 K. The better agreement observed for 5-allyl-1,3-cyclopentadiene at high temperature suggests that the model better account for the formation of the allyl radical. Note that combination products were detected in very small amounts (less than 100 ppm) and that their mole fractions are very sensitive to uncertainties in kinetic parameters.

A comparison of the performance of the new model and that of the initial one is displayed in Supporting Information. The new model performs better for the reactivity and for many reaction products. Particularly for methane, ethylene, allene, 1,3-butadiene, *iso*- and 1-butenes, cyclopentadienyl radical (even if still underestimated by the new model), benzene, toluene, styrene, and indene (still underpredicted). The performance is poorer for some of them. For example, acetylene and naphthalene were better predicted by the original model (but the route of formation for naphthalene was unrealistic in the initial model).

Kinetic Analysis of the Model

A kinetic analysis of the model was performed at a temperature of 1000 K (corresponding to a fuel conversion of 65%). A flux diagram for the consumption of cyclopentene is shown in Figure 9. Cyclopentene is consumed by three types of reactions. It mainly reacts to yield 1,3-cyclopentadiene and a molecule of hydrogen (about 92% of the consumption of cyclopentene). Cyclopentene reacts also by H atom abstraction to give the resonantly stabilized cyclopentenyl radical (about 1%), and it leads to the cyclopentyl radical through H atom addition on the double bond (about 5%).

The cyclopentyl radical (C_5H_9) decomposes by C–C β-scission to yield a linear C_5H_9 radical which in turns decomposes to ethylene and the allyl radical. The cyclopentenyl radical (C_5H_7) undergoes a decomposition by C–H β-scission to yield 1,3-cyclopentadiene (note that overall 93% of cyclopentene transform into 1,3-cyclopentadiene). The 1,3-cyclopentadiene leads to the cyclopentadienyl radical (C_5H_5) through two types of reactions: H atom abstractions (67% of the consumption of C_5H_6) and unimolecular initiation by C–H bond breaking (33% of the consumption of C_5H_6). This radical is the main precursors of aromatics and naphthalene. For a better clarity in Figure 9, the routes of formation of aromatics and naphthalene from C_5H_5 are presented in a global way by dotted arrows. The formation of naphthalene through the sequence of reactions shown in Figure 8 accounts for 52% of the consumption of C_5H_5. The formation of styrene

represents 5% of the consumption of C_5H_5. The formations of benzene is 7% and toluene is less than 1% of the consumption of C_5H_5.

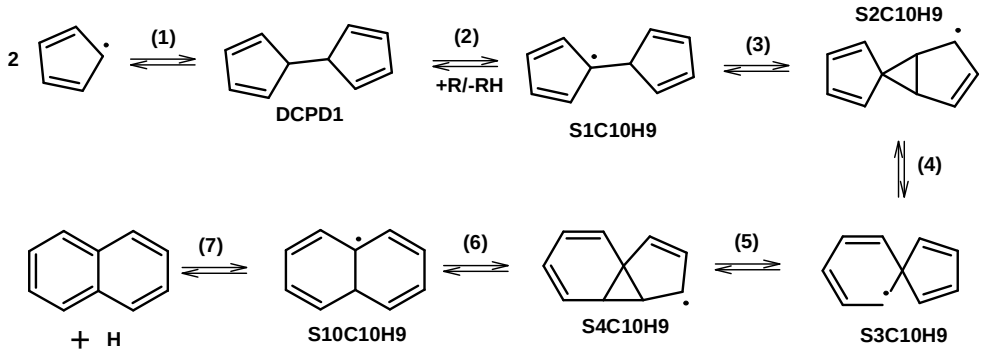

Figure 8. Reactions added in the model to account for the formation of naphthalene (scheme proposed by Kislov and Mebel[17]).

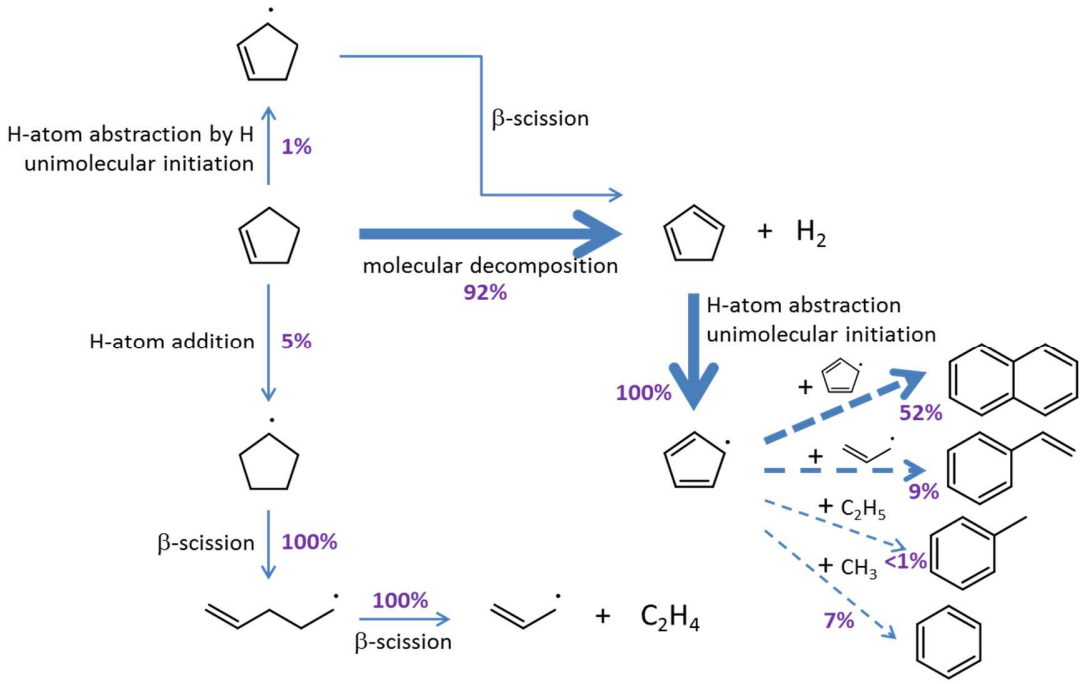

Figure 9. Main consumption routes of cyclopentene (kinetic analysis performed at 1000 K in the conditions of the experimental study).

A sensitivity analysis performed at the same temperature showed that the decomposition of cyclopentene to 1,3-cyclopentadiene is the most sensitive reaction for the consumption of the fuel. The rate constant of this reaction used in the model comes from Lewis et al. ($A = 2.24 \times 10^{13}$ s^{-1} and $Ea = 66.01$ kcal mol^{-1}).[54]

As far as aromatics and naphthalene are concerned, they are mainly formed from the combination of cyclopentadienyl radicals with other radicals present in the gas phase following the schemes which are displayed in Figures 7, 8, S2, and S4 or by addition of the cyclopentadienyl radical to small unsaturated species. The formation of benzene from cyclopentadienyl radicals is 87% whereas the formation of benzene from propargyl radicals (C_3H_3) is only 12%. A sensitivity analysis for the mole fraction of benzene

was performed at 1000 K. The most sensitive reactions are shown in the graph in Figure 10. The reaction which has the most inhibiting effect is the decomposition of the fuel into 1,3-cyclopentadiene and H_2. This can be explained by the fact that the molecular decomposition of the fuel is in competition with other pathways that create more reactive radical species (additions of radical to the double bond and H atom abstractions). Reactions of H atom abstraction consuming propagating radicals (e.g., methyl and allyl radicals) and forming C_5H_5 have also an inhibiting effect in respect to the formation of benzene. The reactions with the most promoting effect is the unimolecular decomposition of 1,3-cyclopentadiene to H + C_5H_5. This can be explained by the fact that the formation of an H atom enhances the overall reactivity of the system and by the fact that C_5H_5 is a precursor of benzene. The H atom abstraction of methylcyclopentadiene (MCPD) by C_5H_5 forming the radical RMCPDY and the reaction of isomerization of RMCPDY to RMCPD have also a promoting effect because they lead to the formation of benzene through the sequence of reactions in Figure 7. The two others pathways that have a promoting effect are the addition of an H atom on the fuel forming the cyclopentyl radical (C_5H_9) which then leads to the formation of the allyl radical (see Figure 9) and the unimolecular decomposition of the fuel that creates two reactive species (an H atom and the resonantly stabilized C_5H_7 radical).

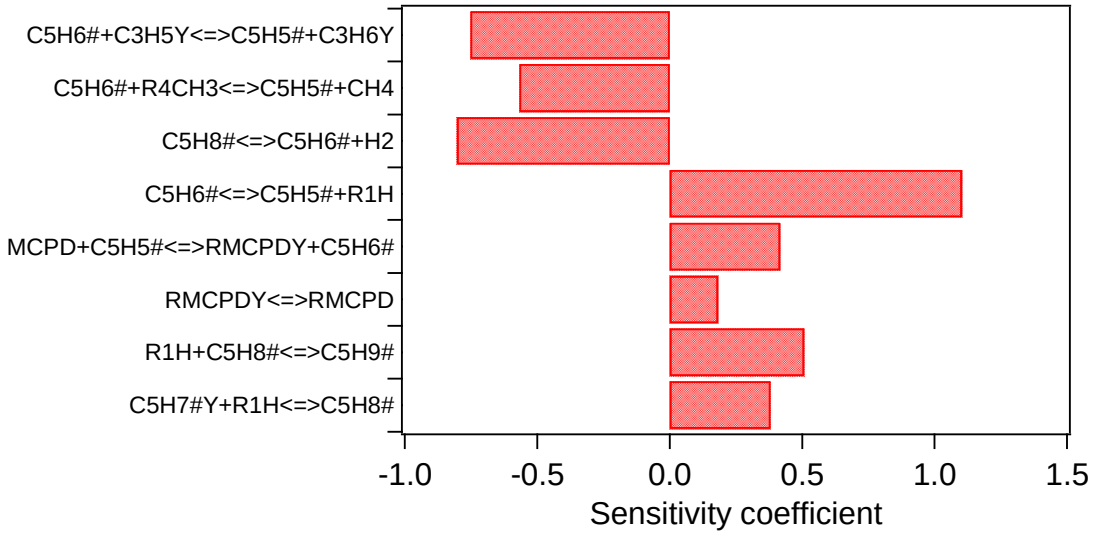

Figure 10. Sensitivity analysis on the benzene mole fraction performed at 1000 K under the conditions of the experimental study.

Conclusion

The thermal decomposition of cyclopentene was studied using a jet-stirred reactor and three complementary analytical methods: gas chromatography, mass spectrometry with ionization by synchrotron radiation, and single photon laser ionization mass spectrometry. Gas chromatography allowed the quantification of 25 products, the main ones being hydrogen and 1,3-cyclopentadiene. SVUV-PIMS data allowed the quantification of the cyclopentadienyl radical (C_5H_5) and proved the absence of fulvene among reaction products. According to photon efficiency spectrum recorded for m/z 78, the second C_6H_6 isomer detected in this work is 1,5-hexadien-3-yne. SPI-MS analyses allowed the detection of two products likely obtained from the combination of allyl and cyclopentadienyl radicals: 5-allyl-1,3-cyclopentadiene and 5-cyclopenta-2,4-diene-cyclopenta-1,3-diene.

The comparison of the three sets of experiment data showed that overall a good agreement in mole fractions obtained with the different analytical method was obtained. Some discrepancies were observed for large aromatics (from styrene) and naphthalene. The gap between the different mole fraction profiles can be attributed to the sampling method which has a significant impact for larger species because of their lower volatility. For these species, the direct sampling in the gas phase seems to provide more reliable results than online gas chromatography.

A model was developed for the pyrolysis of cyclopentene. A new chemistry set for the formation of aromatics from the cyclopentadienyl radical was included in the model. The overall agreement is satisfactory: the conversion of the fuel and the mole fraction profiles of the main reaction product are well reproduced by the model. The formation of benzene and styrene are better reproduced by the model thanks to the inclusion of the new chemistry set whereas the mole fractions of toluene, indene and naphthalene are still under-predicted. There are still a lack of data concerning the formation routes of some species such as 1,5-hexadien-3-yne which is likely an intermediate involved in the formation of benzene. Theoretical studies are needed to elucidate the chemistry of this species.
Supporting Information

Acknowledgment

This work was supported by the European Commission through the “Clean ICE” Advanced Research Grant of the European Research Council and by the COST Actions CM0901 and CM1404.

References

(1) McEnally, C. S.; Pfefferle, L. D.; Atakan, B.; Kohse-Hoeinghaus, K. Studies of Aromatic Hydrocarbon Formation Mechanisms in Flames: Progress towards Closing the Fuel Gap. Prog. Energy Combust. Sci. 2006, 32, 247–294.
(2) Wang, H. Formation of Nascent Soot and Other Condensed-Phase Materials in Flames. Proc. Combust. Inst. 2011, 33, 41–67.
(3) King, K. D. Very Low-Pressure Pyrolysis (VLPP) of Cyclopentene. Int. J. Chem. Kinet. 1978, 10, 117–123.
(4) Burcat, A.; Snyder, C.; Brabbs, T. Ignition Delay Times of Cyclopentene Oxygen Argon Mixtures. In Proc. of the 15th Intl. Symposium on Shock Waves and Shock Tubes; Stanford University Press: Berkeley, 1985; pp 335–341.
(5) McEnally, C. S.; Pfefferle, L. D. An Experimental Study in Non-Premixed Flames of Hydrocarbon Growth Processes That Involve Five-Membered Carbon Rings. Combust. Sci. Technol. 1998, 131, 323–344.
(6) Lamprecht, A.; Atakan, B.; Kohse-Hoinghaus, K. Fuel-Rich Flame Chemistry in Low-Pressure Cyclopentene Flames. Proc. Combust. Inst. 2000, 28, 1817–1824.
(7) Lindstedt, R. P.; Rizos, K.-A. The Formation and Oxidation of Aromatics in Cyclopentene and Methyl-Cyclopentadiene Mixtures. Proc. Combust. Inst. 2002, 29, 2291–2298.
(8) Marinov, N. M.; Pitz, W. J.; Westbrook, C. K.; Vincitore, A. M.; Castaldi, M. J.; Senkan, S. M.; Melius, C. F. Aromatic and Polycyclic Aromatic Hydrocarbon Formation in a Laminar Premixed N-Butane Flame. Combust. Flame 1998, 114, 192–213.
(9) Gueniche, H. A.; Glaude, P. A.; Fournet, R.; Battin-Leclerc, F. Rich Methane Premixed Laminar Flames Doped by Light Unsaturated Hydrocarbons - III. Cyclopentene. Combust. Flame 2008, 152, 245–261.

(10) Hansen, N.; Klippenstein, S. J.; Miller, J. A.; Wang, J.; Cool, T. A.; Law, M. E.; Westmoreland, P. R.; Kasper, T.; Kohse-Hoinghaus, K. Identification of C5Hx Isomers in Fuel-Rich Flames by Photoionization Mass Spectrometry and Electronic Structure Calculations. J. Phys. Chem. A 2006, 110, 4376–4388.
(11) Mulholland, J. A.; Lu, M.; Kim, D.-H. Pyrolytic Growth of Polycyclic Aromatic Hydrocarbons by Cyclopentadienyl Moieties. Proc. Combust. Inst. 2000, 28, 2593–2599.
(12) Kim, D. H.; Mulholland, J. A.; Wang, D.; Violi, A. Pyrolytic Hydrocarbon Growth from Cyclopentadiene. J. Phys. Chem. A 2010, 114, 12411–12416.
(13) Djokic, M. R.; Van Geem, K. M.; Cavallotti, C.; Frassoldati, A.; Ranzi, E.; Marin, G. B. An Experimental and Kinetic Modeling Study of Cyclopentadiene Pyrolysis: First Growth of Polycyclic Aromatic Hydrocarbons. Combust. Flame 2014, 161, 2739–2751.
(14) Dubnikova, F.; Lifshitz, A. Ring Expansion in Methylcyclopentadiene Radicals. Quantum Chemical and Kinetics Calculations. J. Phys. Chem. A 2002, 106, 8173–8183.
(15) Fascella, S.; Cavallotti, C.; Rota, R.; Carrà, S. The Peculiar Kinetics of the Reaction between Acetylene and the Cyclopentadienyl Radical. J. Phys. Chem. A 2005, 109, 7546–7557.
(16) Cavallotti, C.; Mancarella, S.; Rota, R.; Carrà, S. Conversion of C5 into C6 Cyclic Species through the Formation of C7 Intermediates†. J. Phys. Chem. A 2007, 111, 3959–3969.
(17) Kislov, V. V.; Mebel, A. M. The Formation of Naphthalene, Azulene, and Fulvalene from Cyclic C5 Species in Combustion: An Ab Initio/RRKM Study of 9-H-Fulvalenyl (C5H5−C5H4) Radical Rearrangements†. J. Phys. Chem. A 2007, 111, 9532–9543.
(18) Mebel, A. M.; Kislov, V. V. Can the C5H5 + C5H5 → C10H10 → C10H9 + H/C10H8 + H2 Reaction Produce Naphthalene? An Ab Initio/RRKM Study. J. Phys. Chem. A 2009, 113, 9825–9833.
(19) Herbinet, O.; Glaude, P.-A.; Warth, V.; Battin-Leclerc, F. Experimental and Modeling Study of the Thermal Decomposition of Methyl Decanoate. Combust. Flame 2011, 158, 1288–1300.
(20) Herbinet, O.; Marquaire, P.-M.; Battin-Leclerc, F.; Fournet, R. Thermal Decomposition of N-Dodecane: Experiments and Kinetic Modeling. J. Anal. Appl. Pyrolysis 2007, 78, 419–429.
(21) Dagaut, P.; Reuillon, M.; Cathonnet, M. Experimental Study of the Oxidation of N-Heptane in a Jet Stirred Reactor from Low to High Temperature and Pressures up to 40 Atm. Combust. Flame 1995, 101, 132–140.
(22) Husson, B.; Ferrari, M.; Herbinet, O.; Ahmed, S. S.; Glaude, P.-A.; Battin-Leclerc, F. New Experimental Evidence and Modeling Study of the Ethylbenzene Oxidation. Proc. Combust. Inst. 2013, 34, 325–333.
(23) Herbinet, O.; Sirjean, B.; Bounaceur, R.; Fournet, R.; Battin-Leclerc, F.; Scacchi, G.; Marquaire, P.-M. Primary Mechanism of the Thermal Decomposition of Tricyclodecane. J. Phys. Chem. A 2006, 110, 11298–11314.
(24) Matras, D.; Villermaux, J. Un Réacteur Continu Parfaitement Agité Par Jets Gazeux Pour L'étude Cinétique de Réactions Chimiques Rapides. Chem. Eng. Sci. 1973, 28, 129–137.
(25) David, R.; Matras, D. Rules for Construction and Extrapolation of Reactors Self-Stirred by Gas Jets. Can. J. Chem. Eng. 1975, 53, 297–300.
(26) Azay, P.; Côme, G.-M. Temperature Gradients in a Continuous Flow Stirred Tank Reactor. Ind. Eng. Chem. Process Des. Dev. 1979, 18, 754–756.
(27) Herbinet, O.; Dayma, G. Jet-Stirred Reactors. In Cleaner Combustion; Battin-Leclerc, F., Simmie, J. M., Blurock, E., Eds.; Green Energy and Technology; Springer London, 2013; pp 183–210.
(28) Herbinet, O.; Battin-Leclerc, F.; Bax, S.; Gall, H. L.; Glaude, P.-A.; Fournet, R.; Zhou, Z.; Deng, L.; Guo, H.; Xie, M.; et al. Detailed Product Analysis during the Low Temperature Oxidation of N-Butane. Phys. Chem. Chem. Phys. 2011, 13, 296–308.
(29) Qi, F. Combustion Chemistry Probed by Synchrotron VUV Photoionization Mass Spectrometry. Proc. Combust. Inst. 2013, 34, 33–63.
(30) WebBook de Chimie NIST http://webbook.nist.gov/chemistry/ (accessed Oct 3, 2011).

(31) Montgomery Jr., J. A.; Frisch, M. J.; Ochterski, J. W.; Petersson, G. A. A Complete Basis Set Model Chemistry. VI. Use of Density Functional Geometries and Frequencies. J. Chem. Phys. 1999, 110, 2822–2827.
(32) Frisch, M. J.; Trucks, G. W.; Cheeseman, J. R.; Scalmani, G.; Caricato, M.; Hratchian, H. P.; Li, X.; Barone, V.; Bloino, J.; Zheng, G.; et al. Gaussian 09; 2009.
(33) Schissel, P.; McAdoo, D. J.; Hedaya, E.; McNeil, D. W. Flash Vacuum Pyrolysis. III. Formation and Ionization of Cyclopentadienyl, Cyclopentadienyl Nickel, and Dihydrofulvalene (Dicyclopentadienyl) Derived from Nickelocene. J. Chem. Phys. 1968, 49, 5061–5066.
(34) Lossing, F. P.; Traeger, J. C. Stabilization in Cyclopentadienyl, Cyclopentenyl, and Cyclopentyl Cations. J. Am. Chem. Soc. 1975, 97, 1579–1580.
(35) Harrison, A. G.; Honnen, L. R.; Dauben, H. J.; Lossing, F. P. Free Radicals by Mass Spectrometry. XX. Ionization Potentials of Cyclopentadienyl and Cycloheptatrienyl Radicals. J. Am. Chem. Soc. 1960, 82, 5593–5598.
(36) Blocquet, M.; Schoemaecker, C.; Amedro, D.; Herbinet, O.; Battin-Leclerc, F.; Fittschen, C. Quantification of OH and HO2 Radicals during the Low-Temperature Oxidation of Hydrocarbons by Fluorescence Assay by Gas Expansion Technique. Proc. Natl. Acad. Sci. 2013, 110, 20014–20017.
(37) Bieri, G.; Burger, F.; Heilbronner, E.; Maier, J. P. Valence Ionization Energies of Hydrocarbons. Helv. Chim. Acta 1977, 60, 2213–2233.
(38) Backx, C.; Wight, G. R.; van der Wiel, M. J. Oscillator Strengths (10-70 eV) for Absorption, Ionization and Dissociation in H2, HD and D2, Obtained by an Electron-Ion Coincidence Method. J. Phys. B At. Mol. Phys. 1976, 9, 315–331.
(39) Samson, J. A. R.; Stolte, W. C. Precision Measurements of the Total Photoionization Cross-Sections of He, Ne, Ar, Kr, and Xe. J. Electron Spectrosc. Relat. Phenom. 2002, 123, 265–276.
(40) Kameta, K.; Kouchi, N.; Ukai, M.; Hatano, Y. Photoabsorption, Photoionization, and Neutral-Dissociation Cross Sections of Simple Hydrocarbons in the Vacuum Ultraviolet Range. J. Electron Spectrosc. Relat. Phenom. 2002, 123, 225–238.
(41) Mackie, R. A.; Scully, S. W. J.; Sands, A. M.; Browning, R.; Dunn, K. F.; Latimer, C. J. A Photoionization Mass Spectrometric Study of Acetylene and Ethylene in the VUV Spectral Region. Int. J. Mass Spectrom. 2003, 223, 67–79.
(42) Cool, T. A.; Wang, J.; Nakajima, K.; Taatjes, C. A.; McIlroy, A. Photoionization Cross Sections for Reaction Intermediates in Hydrocarbon Combustion. Int. J. Mass Spectrom. 2005, 247, 18–27.
(43) Cool, T. A.; Nakajima, K.; Mostefaoui, T. A.; Qi, F.; McIlroy, A.; Westmoreland, P. R.; Law, M. E.; Poisson, L.; Peterka, D. S.; Ahmed, M. Selective Detection of Isomers with Photoionization Mass Spectrometry for Studies of Hydrocarbon Flame Chemistry. J. Chem. Phys. 2003, 119, 8356–8365.
(44) Zhou, Z.; Xie, M.; Wang, Z.; Qi, F. Determination of Absolute Photoionization Cross-Sections of Aromatics and Aromatic Derivatives. Rapid Commun. Mass Spectrom. 2009, 23, 3994–4002.
(45) Bobeldijk, M.; van der Zande, W. J.; Kistemaker, P. G. Simple Models for the Calculation of Photoionization and Electron Impact Ionization Cross Sections of Polyatomic Molecules. Chem. Phys. 1994, 179, 125–130.
(46) Taatjes, C. A.; Osborn, D. L.; Selby, T. M.; Meloni, G.; Trevitt, A. J.; Epifanovsky, E.; Krylov, A. I.; Sirjean, B.; Dames, E.; Wang, H. Products of the Benzene + O(P-3) Reaction. J. Phys. Chem. A 2010, 114, 3355–3370.
(47) Lifshitz, A.; Tamburu, C.; Suslensky, A.; Dubnikova, F. Decomposition and Ring Expansion in Methylcyclopentadiene: Single-Pulse Shock Tube and Modeling Study. Proc. Combust. Inst. 2005, 30, 1039–1047.
(48) McGivern, W. S.; Manion, J. A.; Tsang, W. Ring-Expansion Reactions in the Thermal Decomposition of Tert-Butyl-1,3-Cyclopentadiene. J. Phys. Chem. A 2006, 110, 12822–12831.

(49) Fascella, S.; Cavallotti, C.; Rota, R.; Carrà, S. Quantum Chemistry Investigation of Key Reactions Involved in the Formation of Naphthalene and Indene. J. Phys. Chem. A 2004, 108, 3829–3843.
(50) Kislov, V. V.; Mebel, A. M.; Aguilera-Iparraguirre, J.; Green, W. H. Reaction of Phenyl Radical with Propylene as a Possible Source of Indene and Other Polycyclic Aromatic Hydrocarbons: An Ab Initio/RRKM-ME Study. J. Phys. Chem. A 2012, 116, 4176–4191.
(51) Kislov, V. V.; Mebel, A. M. An Ab Initio G3-Type/statistical Theory Study of the Formation of Indene in Combustion Flames. II. The Pathways Originating from Reactions of Cyclic C-5 Species - Cyclopentadiene and Cyclopentadienyl Radicals. J. Phys. Chem. A 2008, 112, 700–716.
(52) Koizumi, H. Predominant Decay Channel for Superexcited Organic Molecules. J. Chem. Phys. 1991, 95, 5846–5852.
(53) Person, J. C.; Nicole, P. P. Isotope Effects in the Photoionization Yields and the Absorption Cross Sections for Acetylene, Propyne, and Propene. J. Chem. Phys. 1970, 53, 1767–1774.
(54) Lewis, D. K.; Bergmann, J.; Manjoney, R.; Paddock, R.; Kalra, B. L. Rates of Reactions of Cyclopropane, Cyclobutane, Cyclopentene,and Cyclohexene in the Presence of Boron Trichloride. J. Phys. Chem. 1984, 88, 4112–4116.
(55) Buda, F.; Bounaceur, R.; Warth, V.; Glaude, P. A.; Fournet, R.; Battin-Leclerc, F. Progress toward a Unified Detailed Kinetic Model for the Autoignition of Alkanes from C4 to C10 between 600 and 1200 K. Combust. Flame 2005, 142, 170–186.
(56) Heyberger, B.; Belmekki, N.; Conraud, V.; Glaude, P.-A.; Fournet, R.; Battin-Leclerc, F. Oxidation of Small Alkenes at High Temperature. Int. J. Chem. Kinet. 2002, 34, 666–677.
(57) Sirjean, B.; Glaude, P. A.; Ruiz-Lopèz, M. F.; Fournet, R. Theoretical Kinetic Study of Thermal Unimolecular Decomposition of Cyclic Alkyl Radicals. J. Phys. Chem. A 2008, 112, 11598–11610.
(58) Tsang, W. Mechanism and Rate Constants for the Decomposition of 1-Pentenyl Radicals †. J. Phys. Chem. A 2006, 110, 8501–8509.
(59) Matheu, D. M.; Green, W. H.; Grenda, J. M. Capturing Pressure-Dependence in Automated Mechanism Generation: Reactions through Cycloalkyl Intermediates. Int. J. Chem. Kinet. 2003, 35, 95–119.
(60) Sharma, S.; Green, W. H. Computed Rate Coefficients and Product Yields for c-C(5)H(5) + CH(3) -> Products. J. Phys. Chem. A 2009, 113, 8871–8882.
(61) Burcat, A.; Dvinyaninov, M. Detailed Kinetics of Cyclopentadiene Decomposition Studied in a Shock Tube. Int. J. Chem. Kinet. 1997, 29, 505–514.
(62) Tsang, W. Chemical Kinetic Data-Base for Hydrocarbon Pyrolysis. Ind. Eng. Chem. Res. 1992, 31, 3–8.
(63) Baulch, D.; Cobos, C.; Cox, R.; Esser, C.; Frank, P.; Just, T.; Kerr, J.; Pilling, M.; Troe, J.; Walker, R.; et al. Evaluated Kinetic Data for Combustion Modeling. J. Phys. Chem. Ref. Data 1992, 21, 411–734.
(64) Zhong, X.; Bozzelli, J. W. Thermochemical and Kinetic Analysis of the H, OH, HO2, O, and O-2 Association Reactions with Cyclopentadienyl Radical. J. Phys. Chem. A 1998, 102, 3537–3555.
(65) Mebel, A. M.; Lin, M. C.; Yu, T.; Morokuma, K. Theoretical Study of Potential Energy Surface and Thermal Rate Constants for the C6H5+H2 and C6H6+H Reactions. J. Phys. Chem. A 1997, 101, 3189–3196.